JPET Fast Forward. Published on January 14, 2004 as DOI: 10.1124/jpet.103.062901

JPET #62901

Comparison of Pulmonary/Nasal CYP2F Expression Levels in Rodents and Rhesus Macaque

R. Michael Baldwin[1], William T. Jewell[2], Michelle V. Fanucchi[3], Charles G. Plopper[3], Alan R. Buckpitt[1]

[1]Department of Molecular Biosciences

School of Veterinary Medicine

University of California, Davis

Running Title: CYP2F localization in rodents and rhesus macaque

Corresponding Author: Michael Baldwin

Vet Med: Molecular Biosciences

1311 Haring Hall

UC Davis

Davis, CA 95616

(530) 752-0793 voice

(530) 752-4698 fax

Number of Text Pages: 36

Number of Tables: 1

Number of Figures: 8

Number of References: 29

Word Count Abstract: 249

Introduction: 664

Discussion: 1550

Non-standard Abbreviations:

CYP = Cytochrome P450

CYP2F2 = Cytochrome P4502F2

CYP2F4 = Cytochrome P4502F4

CYP2F = Any or All Members of Cytochrome P4502F family

rCYP2F = Recombinant Cytochrome P4502F isoform

GAPDH = Glyceraldehyde-3-phosphate-dehydrogenase

RFU = relative fluorescence unit

SSC = 150mM NaCl, 15mM Sodium Acetate

SSPE = 150mM NaCl, 10mM NaH_2PO_4, 1mM EDTA

TBST = 12mM Tris, 137mM NaCl, 0.1% Tween-20, pH 7.6

Section Assignment: Toxicology

Abstract

Naphthalene is a ubiquitous environmental contaminant that upon exposure results in dose-dependent and tissue-, species-, and cell-selective necrosis of murine Clara cells. Naphthalene is metabolized by cytochrome P4502F to a 1,2-epoxide; this is the first and obligate step in events leading to cytotoxicity. The studies reported here examine the relationship between levels of transcript (mRNA) and CYP2F protein in the respiratory tract of rodents with tissue susceptibility to injury. In both mice and rats, the lung contains more CYP2F transcript than liver; levels in kidney were undetectable. Mice expressed 4- and 8-fold greater CYP2F transcript in lung and liver tissue, respectively, than rats. Quantitative immunoblot blot analysis of CYP2F in airway subcompartments revealed mice to have 30-(minor daughters/ terminal bronchioles), 20-(major daughter), 40-(trachea), and 6-(parenchyma) fold higher levels of CYP2F protein than rats. Within the lungs of both rodent species, highest CYP2F expression was found in the distal airways. The kidney contained undetectable amounts of CYP2F; multiple immunoreactive reactive bands in liver precluded quantification. The olfactory epithelium contains the greatest amount of CYP protein of all tissues studied in the rat, consistent with the observed pattern of *in vivo* injury. Overall, these studies in rodents demonstrate a strong association between CYP2F expression levels and susceptibility to naphthalene-induced cytotoxicity. Of all primate tissues studied, only the nasal ethmoturbinates contain quantifiable amounts of CYP2F, roughly 10- and 20-fold less than the corresponding tissues in rats and mice, respectively. These results suggest that rhesus macaques may be refractory to naphthalene-induced pulmonary injury.

The environmental toxicant naphthalene can be found in ambient air, ground water, sidestream and mainstream cigarette smoke, and in byproducts from the combustion of diesel fuel (ATSDR, 1995). The toxicological assessment of naphthalene has been the focus of extensive research, and the results of the NTP two-year inhalation studies in mice and rats have found naphthalene to be associated with neoplasia in both species. The inhalation study in mice demonstrated slightly increased incidences of alveolar/bronchiolar adenomas only in females at the highest dose (30 ppm, 156 mg/m^3) (NTP, 1992). In rats, however, neoplasms were confined to the nasal respiratory epithelium and the incidences were dose dependant (NTP, 2000). Previous work has shown that inhalation of naphthalene vapor at levels of 2 ppm (10.5 mg/m^3) and above leads to necrosis of murine pulmonary bronchiolar epithelial cells (West et al., 2001). This exposure concentration is considerably less than the current OSHA exposure standard of 10 ppm (52 mg/m^3) for an 8-hour time-weighted average. These and other data were employed in the recent IARC classification of naphthalene as a possible human carcinogen (IARC, 2002). Given the extent to which naphthalene is found in the environment, the likelihood of human exposure and the body of evidence demonstrating its toxicity in animal models, understanding the mechanism of toxic injury is essential. Elucidation of the factors most clearly associated with susceptibility to injury in animal models will allow far better assessments of human risk to be developed.

The ability of the lung to metabolize several protoxicants has been well established. Compounds such as 4-ipomeanol, trichloroethylene, 1-nitronaphthalene, 3-methylindole, and naphthalene undergo metabolic activation by monooxygenases (CYP) leading to the injury of lung epithelial cells (reviewed in Gram, 1997). Within the heterogeneous population of more than 40 cell types in the lung, the non-ciliated bronchiolar epithelial (Clara) cells are especially sensitive to injury,

and this sensitivity correlates with the localization of CYP enzymes in this cell type. However, substantial differences have been observed in the sensitivity of this cell population across species. For example, parenteral administration of naphthalene, and of trichloroethylene resulted in Clara cell necrosis in the lungs of mice but not rats (Plopper, 1993). In rats, injury was confined to the nasal olfactory epithelium after parenteral administration of naphthalene at doses substantially less than the LD50. These observations could be explained by relative differences in species specific CYP catalytic activities and/or the relative cellular CYP expression levels of mice and rats.

Naphthalene is metabolized to naphthalene 1,2-epoxide, a reactive intermediate, by the CYP system. Both the 1S,2R- and the 1R,2S- stereoisomers are produced. This biotransformation is the first and obligate step in the cascade of events leading to toxic injury. In preparations of microsomes or airway explants from lungs of mice, naphthalene epoxide formation occurs with a high degree of stereoselectivity, with ratios of 1R,2S- to 1S,2R- epoxide of 10:1 and >25:1, respectively (Buckpitt et al., 1992, 1995). In rats, both the absolute rate and the degree of stereoselectivity of epoxidation are significantly less than in mice. Previous work has shown the presence of CYP2F2 in murine Clara cells to correlate with the stereoselectivity and rate of naphthalene metabolism and to the site of injury (Buckpitt et al., 1995). Co-incubation of an inhibitory CYP2F2 antibody dramatically decreases the formation of the 1R,2S-naphthalene epoxide in murine lung microsomal incubations (Nagata et al., 1990). Using recombinant CYP2F2 (rCYP2F2) expressed in insect cells, Shultz et al. (1999) found naphthalene to be rapidly metabolized with a very high degree of stereoselectivity for the 1R,2S configuration, strongly suggesting the generation of this metabolite to be an important determinant of

susceptibility.

This study addresses the relationship between the amount of transcript (mRNA), protein expression levels, and the catalytic activity of a reactive metabolite generating enzyme (CYP2F) with *in vitro* metabolism and ultimately, the extent and localization of cytotoxic injury observed *in vivo*. Accordingly, we have shown that species susceptibility to naphthalene toxicity is associated with clear differences in relative cellular expression levels of the CYP2F protein.

Methods

Rodents

Adult male Sprague-Dawley rats (225-250g) and male Swiss-Webster mice (25-30g) were purchased from Charles River Laboratories (Wilmington, MA). The animals were housed in an AAALAC-accredited facility in cage racks supplied with high-efficiency particulate filtered air and inert bedding. Animals had free access to food (Purina Rodent Chow) and water, with a 12-hr/12-hr light/dark cycle for at least 7 days before use. Rodents were killed with an overdose of sodium pentobarbital administered ip**.**

Northern Blot Analysis

Total RNA was isolated from lung, liver, and kidney of four mice and four rats using Trizol reagent (Invitrogen, Carlsbad, CA). RNA from rat (20 μg) and mouse (5 μg) was separated on 1% agarose gels and transferred to positively charged nylon membranes according to the manufacture's instructions (NorthernMax-Gly, Ambion, Austin, TX). cDNA probes were generated by RT-PCR of total RNA from rat lung; the CYP2F4 probe (1409bp (26..1434) accession# AF017393) was 93% homologous to CYP2F2; the rat GAPDH probe (849bp (152..1000) accession# M17701) was 95% homologous to the mouse transcript. Probes were ^{33}P-labeled using a Decaprime II DNA labeling kit (Ambion) and blots were hybridized at a concentration of $2.5x10^6$cpm/ml overnight at 42 °C in hybridization buffer (5x SSPE, 50% formamide, 0.5% SDS, 4x Denhardt's solution, 100 μg/ml salmon sperm DNA). Following stringent washing with SSC, blots were developed with storage phospor screens (Amersham Biosciences, Piscataway, NJ) scanned with a Typhoon 8600 (Amersham Biosciences) and bands were quantified using ImageQuant 5.1 software (Amersham Biosciences).

Immunoblotting of Rat and Mouse Tissues

Airway segments were microdissected from lungs according to methods previously described in detail (Plopper et al., 1991). Briefly, animals were killed and tracheas were cannulated. Lungs were infused with 1% low-melting point agarose (Seaplaque, FMC, Rockland, ME) in Waymouth's medium containing protease inhibitors (Cocktail Set III, CalBiochem, San Diego, CA) and then immediately cooled on ice in Waymouth's medium. Kidneys and liver were removed and snap frozen in liquid nitrogen and stored at -80 ºC until processed. Airways were blunt dissected under a dissecting microscope to obtain distal trachea, major and minor daughter bronchi, terminal bronchioles, and parenchyma. The collected tissue samples were snap frozen in liquid nitrogen, and stored at -80 °C. Nasal compartments were microdissected as previously described (Fanucchi et al., 1999). The head of each rodent was removed from the carcass, the lower jaw and skin were removed, and the head was split in half along the medial suture. The septum, maxilloturbinates, nasoturbinates, and ethmoturbinates were removed by careful blunt dissection.

Kidney and liver tissue were homogenized on ice using a rotor/stator (Virtishear, Virtis, Gardiner, NY) in phosphate buffer (100mM, pH 7.4 with protease inhibitors). The crude homogenates were centrifuged for 20 minutes at 10,000 x g (4 °C) and the post mitochondrial supernatants were used for immunoblotting. To each sample of lung or nasal tissue, 100 µl of 2x treatment buffer (0.125 M Tris-Cl pH 6.8, 4% SDS, 20% glycerol, 10% 2-mercaptoethanol) was added. Samples were heated to 70 °C for 10 min, sonicated twice for 20 sec, placed at 70 °C for an additional 10 minutes, then centrifuged at 15,000 x g for 30 minutes at ambient

temperature. The supernatant was used for immunoblotting. The limited quantities of respiratory protein available necessitated the use of a fluorescent assay with increased sensitivity for determining total protein concentrations (NanoOrange, Molecular Probes, Eugene, OR). The increased sensitivity allowed for adequate sample dilution to minimize interference with the assay from the buffer constituents.

Proteins were separated by SDS-PAGE using 1mm 10% Bis-Tris gels (Invitrogen). Gels were wet transferred (Mighty Small Transphor, Amersham Biosciences) to PVDF membrane (Immobilon-P^{sq}, Millipore, Bedford, Mass) in transfer buffer (25mM Tris, 192mM glycine, 20% methanol, 0.05% SDS) and then incubated in 5% powdered milk at 4 °C overnight (BioRad, Hercules, CA). The CYP2F isoforms were detected using rabbit anti-CYP2F2 (Nagata et al., 1990) diluted 1:20,000 and chemiluminescent detection according to the manufacturer's directions (ECL plus, Amersham Biosciences) with the following modifications: the goat anti-rabbit secondary antibody was diluted 1:100,000; after the final TBST rinse, membranes were placed in a resealable bag (#402, Kapak, Minneapolis, MN); 1 mL of ECL substrate was applied directly to the blot and then placed in the dark. Two hours later, blots were analyzed with a Storm 860 fluorescence scanner (Amersham Biosciences) in blue mode (≈450nm LED) with a PMT voltage of 850mV and a resolution of 100μm. Bands were quantified using ImageQuant 5.1 (Amersham Biosciences).

Prior to the determination of relative CYP2F protein expression between species, the ability of the rabbit anti-CYP2F2 polyclonal antibody to recognize both CYP2F2 and CYP2F4 was compared semi-quantitatively. Similar amounts of both recombinant CYP2F2 (Shultz et al.,

1999) and CYP2F4 (Baldwin, unpublished results) protein were electrophoresed on two identical gels, one of which was stained with Sypro Ruby (Molecular Probes) and the other immunoblotted as described above. The Sypro Ruby-stained gel was scanned on a Typhoon 8600 scanner, using a 532nm excitation wavelength, a 610BP30 emission filter, a PMT voltage of 600mV and a resolution of 50µm. Quantitations were based on the assumption that fluorescent signal areas were proportional to the amount of recombinant protein present in each lane. By determining the relative amount of recombinant protein per nanogram of cell lysate protein for the two expressed CYP2F isoforms, immunoblot signal intensities could then be normalized for differences in expression levels and compared. Relative fluorescent areas versus nanogram of insect cell lysate protein for each CYP2F isoforms were plotted for both the Sypro Ruby stained gel and the immunoblot (Fig. 2A and 2B). For an equally crossreactive antibody, the relationship of RFU / ng protein (plot slope) between the cell lysates containing either of the two recombinant proteins would be the same on plots of both the immunoblot and Sypro Ruby stained gel.

To allow for the comparison of CYP2F protein expression level across samples from multiple blots, four protein standard solutions were made, using either pooled mouse terminal bronchiole tissue or recombinant CYP2F4 which were diluted 2, 4, and 8 fold. These four standards were run with every immunoblot, and the relative fluorescent units of each band were plotted versus dilution factor. From the linear regression analysis of these points, band intensities could readily be normalized across membranes. Additionally, this method allowed for assessing appropriate sample dilution as well as for recognizing aberrant experiments.

Rhesus Macaque Immunomapping

Through a collaborative effort, samples of respiratory tissue from young adult rhesus macaques used as untreated controls from studies conducted at the University of California Regional Primate Research Center (Davis, CA) were obtained over a series of several months. In all cases, the tissues obtained during necropsy were placed temporarily on ice until snap frozen in liquid nitrogen and stored at -80 °C. Airway segments (trachea, proximal and medial conducting airways, respiratory bronchioles, and parenchyma) and nasal subcompartments (septum, maxilloturbinates, nasoturbinates, and ethmoturbinates) were processed identically to the rodent tissues described above.

Electrophoresis and Immunoblotting of Ethmoturbinate Microsomes from Mice, Rats, and Monkeys

Ethmoturbinate microsomes from mice, rats, and rhesus macaques were prepared by differential centrifugation according to established methodology (Schenkman and Jansson, 1999). To allow for sufficient amounts of microsomal protein, ethmoturbinate tissue was pooled from several animals of each species [mice (8), rat (4), monkey (4)]. Using two identical medium format (140 x 1.5mm) 7% tris-glycine polyacrylamide gels (Duracryl, Genomic Solutions, Ann Arbor, MI), ethmoturbinate microsomal proteins were electrophoresed in duplicate. In a fashion analogous to the antibody crossreactivity experiment, the protein in one gel was stained (Coomassie blue in this instance) and the other immunoblotted as described above with one addition. After being electroblotted, the nylon membrane was briefly rinsed with water and then stained with Coomassie blue (0.1% brilliant blue R250, 1% glacial acetic acid, 50% methanol). After adequate destaining in 50% methanol, proteins could be visualized and assessed for adequate

resolution and protein transfer. The location of the molecular weight markers were etched in pencil on the nylon membrane. Following a quick methanol rinse (≈30 sec) to remove the bulk of remaining stain, the membrane was rinsed twice with TBST (5 minutes) and placed in 5% powdered milk-TBST. Immunodetection was then performed as described above.

Identification of Proteins by Peptide Mass Fingerprinting

In order to accurately obtain the Coomassie-stained bands corresponding to the immunoreactive bands observed on the immunoblot of the duplicate gel, each sample of ethmoturbinate microsomal protein was electrophoresed with a molecular weight marker in both adjacent lanes (Fig. 8). Three protein standard bands were then used to align each immunoreactive band observed in the immunoblot with the Coomassie-stained gel. To assist with this, a digital image of the scanned immunoblot was printed on a plastic transparency and placed beneath the Coomassie-stained gel. Each band was excised with a clean surgical blade.

Excised protein bands were washed thoroughly four times with Milli-Q (Millipore, MA) water. The protein band was diced into approximately 1mm squares and dried in a vacuum centrifuge. Proteins were reduced and alkylated according to an established procedure (Shevchenko et al, 1996). Briefly, proteins were reduced with 10 mM dithiothreitol in 100 mM NH_4HCO_3 (pH 8, 55 ^oC) for 1 h, then alkylated with 55 mM iodoacetamide in 100 mM NH_4HCO_3 for 45 min in the dark at room temperature. Excess reagent was removed, and gel pieces were washed with 100 mM NH_4HCO_3 and partially dehydrated with acetonitrile; complete dehydration was then done in a vacuum centrifuge. Finally, proteins were digested in 50 mM NH_4HCO_3 containing sequencing-grade, modified trypsin (Promega, Madison, WI) at a final trypsin concentration

range of 10 to 25 ng/µl (37 ^{o}C) for 17 h. Peptides were extracted once each with 0.1% trifluoroacetic acid and then 5% formic acid in 50% acetonitrile. The volume was then decreased to 15 µl for mass spectrometric analysis by use of the vacuum centrifuge.

Tryptic peptides were analyzed with a Bruker Biflex III MALDI-TOF mass spectrometer (Bruker-Franzen Analytik, Bremen, Germany) equipped with a pulsed N_2 laser (337nm), a delayed extraction ion source and a reflectron. Fractions of tryptic peptides were desalted using C18 ZipTips (Millipore, Bedford, MA). Peptides were eluted from the ZipTip with 0.1% trifluoroacetic acid-acetonitrile (50:50). Next, 0.5 µl of the peptide aliquot (eluant) was mixed with an equal volume of matrix solution (a saturated solution of α-cyano-4-hydroxycinnamic acid in 0.1% trifluoroacetic acid-acetonitrile (50:50)) and applied to the target. The mass spectra were acquired in the reflectron mode. Due to the number and intensity of peaks in each mass spectrum, trypsin autolysis peaks (842.5 and 2211.1 Da) were obscured. Instead, internal mass calibration was performed by spiking samples with three peptide internal standards of masses 842.51, 1046.54 and 3148.47 Da. This procedure typically results in mass accuracies of 50 ppm or better. Measured monoisotopic masses of tryptic peptides were used as inputs to search the corresponding species databases (Swiss-Prot 9/19/03 release and NCBI 9/1/03) using both the Profound (http://129.85.19.192) and EXPASY (http://us.expasy.org) search engines. The constraints of a 50 ppm mass accuracy, a molecular weight range from 50-62kD (≈56kD±10%) and zero missed tryptic cleavage sites were used for all searches. The Profound search engine was used iteratively; protein matches were accepted based on highest probability followed by subtraction of the "matched" peptides and repeating the process with the remaining peptides. Given the high sequence homologies between CYP enzymes from humans and the rhesus

macaque and the limited protein sequence data presently available for the rhesus macaque, all CYP isoforms identified in the rhesus macaque correspond to matches with tryptic fragments from human CYP isoforms.

Results

Northern Blot Analysis of CYP2F Transcript in Rodents

Prior to comparing the relative CYP2F transcript levels in lung, liver, and kidney of mice and rats (Fig. 1), the expression patterns of two commonly used "housekeeping" genes, β-actin and GAPDH, were compared across species and tissue types in a subset of samples. For a given tissue type, similar GAPDH signal/μg total RNA ratios were observed regardless of species. Ratios varied more than five fold between tissue types (data not shown). Because the β-actin and CYP2F transcripts differed only by approximately 100bp, CYP2F expression levels were normalized to GAPDH expression. Initially, several cDNA probes of differing lengths were compared for specificity and sensitivity to differences in sequence homology across species. The 1409bp CYP2F4 probe and a 849bp rat GAPDH probe were found to be the least affected by differences in hybridization affinities across species and demonstrated acceptable specificity. Negligible differences were observed when northern analysis was repeated using analogous probes made from mouse genes (data not shown).

Highest signal intensities for CYP2F transcript were observed in mouse lung and to a lesser extent in mouse liver (Fig. 1). A similar trend was observed in the rat which, compared to mouse, expressed four-fold and eight-fold less CYP2F transcript in lung and liver tissue, respectively. Negligible amounts of CYP2F transcript were detected in the kidney of either species.

Species Differences in CYP2F Protein by Immunoblot Analysis

Using recombinant proteins as standards, the polyclonal anti-CYP2F2 antibody was estimated to have comparable affinities for rCYP2F2 and rCYP2F4 (Fig. 2). The system of ECL and fluorescent scanning was reproducible, linear over a 50-fold range, and all samples were diluted appropriately to concentrations within the linear concentration range. No signal was observed on immunoblots prepared from the kidney of either rat or mouse. In contrast, multiple poorly resolved but reproducible immunoreactive protein bands precluded the comparison of hepatic CYP2F protein levels across species (Fig. 3).

A representative immunoblot of minor daughter airway proteins from mice and rats along with the four protein standards shows that the antibody recognizes a single 50-52 kD protein in mouse airway when relatively small amounts of protein (1.5 µg) were electrophoresed (Fig. 4). In comparison, several proteins of lower molecular weight, in addition to CYP2F4, were observed in rat airways when 20-fold higher amounts of protein were loaded onto the gel. However, within all areas of lung tissue studied, a single immunoreactive protein with an apparent molecular weight identical to rCYP2F4 was observed within the molecular weight range of 40 to 60 kD.

Immunoblot analysis of proteins from nasal tissues revealed a significantly smaller differential between CYP2F expression levels in mice and rats. Additionally, in many instances, two immunoreactive bands having apparent molecular weights consistent with potential crossreactivity with other cytochrome P450 enzymes were observed (Fig. 5). Although the

proteins from rat nasal tissues demonstrated this "double-banding" pattern to a lesser extent than did corresponding samples from mice, the ethmoturbinates of both species yielded the most distinctive "double-banding" of all nasal areas studied. No additional immunoreactive bands were observed outside the molecular weight ranges shown in Figure 5. The relative CYP2F expression levels of all respiratory tissues studied in mice and rats are summarized in Figure 6.

Immunoblot Analysis of CYP2F in Monkey Lung and Nasal Epithelium

Immunoblot analysis of proteins from all airway levels of the rhesus macaque tested at the highest protein loads (30 µg) failed to detect any trace of an immunoreactive protein using the rabbit anti-CYP2F2 polyclonal antibody (data not shown). Similar results were observed in the nasal and maxilloturbinates, as well as in two of the three septal samples. Interestingly, there were readily detectable and quantifiable levels of a single immunoreactive protein with an apparent molecular mass identical to rCYP2F4 in the protein samples from ethmoturbinates (Fig. 7). Using mean values, the amount of immunoreactive protein in the ethmoturbinate of the rhesus macaque was 10- and 20-fold less than from the ethmoturbinates of rats and mice, respectively. The limit of detection for all monkey samples tested was a factor of four below the values observed in the ethmoturbinates.

Peptide Mass Fingerprinting of Ethmoturbinate Microsomal Proteins

Figure 8 shows the SDS-PAGE separation of proteins stained with Coomassie blue from the ethmoturbinates of mouse, rat, and monkey aligned with the immunoblot of the duplicate gel. The two immunoreactive bands in the mouse and rat aligned well with two intensely stained areas on the Commassie stained gel, whereas the single band observed in monkey aligned with

an area of diffuse Coomassie staining. To determine whether the immunoblotting results properly represented the quantity of CYP2F in the sample or whether crossreactivity with other CYP2 proteins was leading to the observed signal, bands on the gel marked with lines in Figure 8 were excised and digested with trypsin for peptide mass fingerprinting as described above in Methods. Table 1 lists all cytochrome P450s with more than five unique matches from the 60-100 peptide fragments detected in each gel slice by MALDI-TOF mass spectrometry. For both mice and rats, the predominant P450 proteins observed in the upper immunoreactive band were CYP2A and CYP2G1. The lower band was found to contain CYP2F with some signal associated with CYP2A. Monkey ethmoturbinate microsomes contained CYP2A, and the presence of CYP2J2 and CYP2F are strongly suggested (listed in Table 1 as tentative identifications).

Discussion

Previous work demonstrating a strong correlation between CYP2F2 expression in mouse airways and naphthalene toxicity, suggests insensitivity of the rat may result from differences in the catalytic activity of the rat orthologue, CYP2F expression levels, or a combination of both. Although the rat is insensitive to naphthalene-induced pulmonary injury, rat nasal epithelium is a target after either long-term inhalation (NTP, 2000) or single dose parenteral administration (Plopper et al., 1992). However, unlike lung, where previous immunohistochemical studies have provided qualitative information on CYP2F expression patterns in mice and rats, little is known about CYP2F expression levels in nasal epithelium. The data presented here demonstrate significant differences in CYP2F transcript and protein levels within the respiratory tract of these two rodent species. Extension of these studies to the rhesus macaque reveals an even greater differential in CYP2F expression.

Comparison of CYP2F transcript levels from mouse and rat lung revealed trends consistent with the species and tissue selectivity of naphthalene-induced injury *in vivo*. Both species displayed higher levels of transcript in lung compared to liver, and murine tissue contained greater amounts than the corresponding rat tissue. Similar results were observed by Nhamburo et al. (1990), who reported greater amounts of CYP2F transcript in rat lung than liver. In comparison to the four-fold rodent species difference observed in the current studies, Ritter et al. (1991) reported a dramatic 50-fold higher level of CYP2F mRNA in mouse versus rat lung and a 5-10 fold greater amount of transcript in rat liver versus rat lung.

The four-fold difference between mouse and rat CYP2F transcript levels in whole lung observed in the current work are consistent with the differential observed in immunoblots of parenchymal tissue. Since conducting airway epithelial cells account for only 5% of the total cell population in rat lung (Mercer et al., 1994), and alveolar cells comprise 74% (Stone et al., 1992), distal sections of whole lung are likely most similar to parenchymal tissue.

Using the anti-CYP2F2 antibody, comparison of airway subcompartments across species showed that mice had 30- (minor and terminal bronchi), 20- (major daughter), 40- (trachea), and 6- (parenchyma) fold higher levels of immunoreactive CYP2F than rats (Fig. 6). These trends agree with data demonstrating higher rates of naphthalene metabolism in airways of mice than rats (Buckpitt et al., 1995). The distribution of CYP2F within the respiratory tract is similar in both species. In mice, highest CYP2F expression was found in distal airways, with trachea, more proximal airways, and parenchyma having 86%, 36%, and 4% of the expression found in terminal bronchioles, respectively. This distribution is consistent with previous immunohistochemical studies in mice (Buckpitt et al., 1995). The minimal anti-CYP2F2 staining observed in previous studies of rat airways can be attributed to limited sensitivity, since lung areas with greatest CYP2F abundance were 30-fold less than the corresponding mouse tissue. Although immunohistochemical studies only allow for approximation of differences in CYP2F expression, cells containing an immunoreactive epitope could be visualized within the unique population of cell types in each lung subcompartment. While the present methodology is considerably more sensitive and quantitative than immunohistochemical approaches, perceived differences in CYP2F signal between species are potentially attributable to both increased CYP2F expression per cell and differences in the percentage of CYP2F expressing cells within

the region sampled. For example, although the trachea was not found to express large amounts of CYP2F in either rats or mice, the greatest relative difference across species was observed in this location. Clara cells make up a larger percentage of the tracheal epithelial cell population in mice than in rats, likely contributing to the observed differential in CYP2F expression (Plopper, 1993).

The observation of two immunoreactive bands in the rodent olfactory epithelium necessitated further studies to determine the location of CYP2F and to characterize other crossreacting isoforms. Peptide mass fingerprinting of ethmoturbinate proteins corresponding to the two immunoreactive bands yielded fragment matches consistent with CYP2A, CYP2G1, and CYP2F. The upper (≈54kDa) immunoreactive band contained the largest number of peptide fragments from CYP2A, and the only positive identification for CYP2G1. CYP2F was found exclusively in the lower (≈50kDa) band along with fragments corresponding to CYP2A. Fewer fragments for CYP2A were observed in the lower band compared to the upper band. These findings agree with previous studies suggesting that CYP2A5 and CYP2G1 isoforms account for up to 35% of olfactory mucosal P450 content in mice (Gu et al., 1998). The sequence homologies of CYP2A5 and CYP2G1 with CYP2F2 (52% and 55%, respectively), suggest that crossreactivity is likely. Although the present methodology has some limitations, it allows for the determination of the predominant nasal CYP isoforms and provides a basis for quantifying the appropriate immunoreactive band associated with CYP2F. However, the number of peptide fragments generated from numerous proteins in each gel slice precludes the development of a complete picture of the content of nasal CYP isoforms. Only three CYP isoforms present in rodent olfactory epithelium (reviewed in Thornton-Manning and Dahl, 1997a) were identified.

The greatest amount of CYP2F was observed in the ethmoturbinates and maxilloturbinates of both rodent species. Similarly, immunohistochemical studies have localized CYP2A3 in both olfactory and respiratory epithelia of the rat (Thornton-Manning et al., 1997b). In comparison, CYP2G1 protein is present exclusively in the olfactory epithelium of both mouse (Hua et al., 1997) and rat (Zupko et al., 1991).

Within each rodent species, comparison of relative CYP2F protein expression levels in the nasal epithelium and tracheobronchial airways revealed expression patterns consistent with both *in vitro* metabolism studies and cell injury observed *in vivo*. In contrast to the lung where mouse/rat differences in CYP2F expression are dramatic, values observed in the nasal epithelia of mice and rats were more similar, making explanation of tissue susceptibility less obvious. Although observation of two-fold greater amounts of CYP2F protein in murine nasal epithelia is consistent with previous metabolism studies (Buckpitt et al., 1995), it fails to explain the higher susceptibility of rat nasal olfactory epithelium compared to mouse. The reason for the lack of correlation between catalytic activities and levels of CYP2F protein with the susceptibilities observed in the olfactory epithelium of these rodent species is unclear. Potential explanations include: (1) more naphthalene (parent compound) reaches the olfactory epithelium of the rat, (2) other P450 enzymes are important in naphthalene activation in the rat, or (3) differences in olfactory detoxification mechanisms (ex. glutathione levels) exist across these species.

Given the strong association between CYP2F expression levels and susceptibility to naphthalene-induced cytotoxicity demonstrated in rodents, studies were extended to the rhesus

macaque, a species having similar pulmonary physiology and morphology to the human. Of all the tissues tested in the rhesus macaque, only the ethmoturbinates yielded CYP2F signal. In contrast to the two distinct bands observed in rodents (Fig. 8), ethmoturbinate microsomal proteins from the rhesus macaque contained a single diffuse immunoreactive band. To confirm the identity of the immunoreactive ethmoturbinate protein(s), peptide mass fingerprinting was utilized. Analysis of the wide area around the single immunoreactive band yielded tryptic fragments matching CYP2A13/2A6 and potentially CYP2J2 and CYP2F. The compliment of CYPs identified here along with the absence of CYP2G1, is nearly identical to the human olfactory epithelium (Su et al., 2000 and Gu et al., 2000). Although the peptide mass fingerprinting methodology employed is not considered quantitative, our observation of more CYP2A13-specific peptide fragments compared to CYP2A6 is consistent with quantitative RT-PCR results demonstrating CYP2A13 transcript to be more abundant than CYP2A6 in the human olfactory epithelium (Chen et al., 2003).

Quantification of the immunoreactive band observed in monkey ethmoturbinate tissue as CYP2F was based on: 1) an apparent molecular weight identical to rCYP2F standards, 2) peptide mass fingerprinting demonstrating CYP2A3 and CYP2A5 to have larger apparent molecular weights than rCYP2F standards, 3) identification of two unique tryptic fragments consistent with a CYP2F isoform, and 4) identification of a monkey ethmoturbinate CYP2F transcript (mRNA) using RT-PCR (unpublished results). Assuming a reasonably crossreactive antibody, a conservative immunoblot limit-of-detection estimate provides that all areas devoid of CYP2F signal have more than a 40- or 160-fold differential in CYP2F expression compared to rat ethmoturbinates or mouse terminal bronchioles. Even if CYP2F is entirely absent from this

primate species and the signal observed in ethmoturbinates is due to crossreactivity with CYP2A, the conclusion that there are dramatic rodent/primate differences in CYP2F expression remains unchanged.

Lung microsomal incubations have demonstrated the rhesus macaque to metabolize naphthalene at a rate roughly 100- and 10-fold less than mice and rats (Buckpitt et al., 1992). Those data and the data presented here demonstrating no detectable CYP2F in any of the lung subcompartments tested, suggest the rhesus macaque to be refractory to naphthalene-induced pulmonary toxicity. Even though assessment of nasal susceptibility is less clear, the magnitude of the rhesus-to-rodent differential in olfactory CYP2F expression would also suggest a lack of susceptibility for the monkey.

The low rates of naphthalene metabolism observed in human lung microsomes (Buckpitt and Bahnson, 1986) and in the rhesus macaque (Buckpitt et al., 1992), suggest that rodents do not accurately predict human pulmonary response to naphthalene exposure. Ongoing kinetic studies using rodent and rhesus nasal microsomes, and isolated airway segments of the rhesus, are designed to provide additional comparative data for extrapolating the potential toxicity of naphthalene in humans. Ultimately, unequivocal determination of primate susceptibility to naphthalene will require *in vivo* testing and ascertainment of pulmonary and nasal injury.

References

Agency for Toxic Substances and Disease Registry (ATSDR) (1995) *Toxicological Profile for Naphthalene, 1-Methylnaphthalene, 2-Methylnaphthalene,* pp 1-200, ATSDR, Atlanta.

Buckpitt AR and Bahnson LS (1986) Naphthalene metabolism by human lung microsomal enzymes. *Toxicology* **41**:333-341.

Buckpitt A, Buonarati M, Avey LB, Chang AM, Morin D and Plopper CG (1992) Relationship of cytochrome P450 activity to Clara cell cytotoxicity. II. Comparison of stereoselectivity of naphthalene epoxidation in lung and nasal mucosa of mouse, hamster, rat and rhesus monkey. *J Pharmacol Exp Ther* **261**:364-372.

Buckpitt A, Chang AM, Weir A, Van Winkle L, Duan X, Philpot R and Plopper C (1995) Relationship of cytochrome P450 activity to Clara cell cytotoxicity. IV. Metabolism of naphthalene and naphthalene oxide in microdissected airways from mice, rats, and hamsters. *Mol Pharmacol* **47**:74-81.

Chen Y, Liu YQ, Su T, Ren X, Shi L, Liu D, Gu J, Zhang QY and Ding X (2003) Immunoblot analysis and immunohistochemical characterization of CYP2A expression in human olfactory mucosa. *Biochem Pharmacol* **66**:1245-1251.

Fanucchi MV, Harkema JR, Plopper CG and Hotchkiss JA (1999) In vitro culture of microdissected rat nasal airway tissues. *Am J Respir Cell Mol Biol* **20**:1274-1285.

Gram TE (1997) Chemically reactive intermediates and pulmonary xenobiotic toxicity. *Pharmacol Rev* **49**:297-341.

Gu J, Zhang QY, Genter MB, Lipinskas TW, Negishi M, Nebert DW and Ding X (1998) Purification and characterization of heterologously expressed mouse CYP2A5 and CYP2G1: role in metabolic activation of acetaminophen and 2,6-dichlorobenzonitrile in mouse olfactory mucosal microsomes. *J Pharmacol Exp Ther* **285**:1287-1295.

Gu J, Su T, Chen Y, Zhang QY and Ding X (2000) Expression of biotransformation enzymes in human fetal olfactory mucosa: potential roles in developmental toxicity. *Toxicol Appl Pharmacol* **165**(2):158-162.

Hua Z, Zhang QY, Su T, Lipinskas TW and Ding X. (1997) cDNA cloning, heterologous expression, and characterization of mouse CYP2G1, an olfactory-specific steroid hydroxylase. *Arch Biochem Biophys* **340**:208-214.

International Agency for Research on Cancer (IARC) (2002) Monographs on the evaluation of carcinogenic risks to humans: some traditional herbal medicines, some mycotoxins, naphthalene and styrene. Vol 82, IARC, Lyons.

Mercer RR, Russell ML, Roggli VL and Crapo JD (1994) Cell number and distribution in human and rat airways. *Am J Respir Cell Mol Biol* **10**:613-624.

Nagata K, Martin BM, Gillette JR and Sasame HA (1990) Isozymes of cytochrome P-450 that metabolize naphthalene in liver and lung of untreated mice. *Drug Metab Dispos* **18**:557-564.

National Toxicology Program (1992) Toxicology and Carcinogenesis Studies of Naphthalene (CAS No. 91-20-3) in B6C3F$_1$ Mice (Inhalation Studies), in *NTP Technical Report No. 410; NIH publication No. 92-3141*, Research Triangle Park.

National Toxicology Program (2000) Toxicology and Carcinogenesis Studies of Naphthalene (CAS No. 91-20-3) in F344/N Rats (Inhalation Studies), in *NTP Technical Report No. 500; NIH publication No. 01-4434*, Research Triangle Park.

Nhamburo PT, Kimura S, McBride OW, Kozak CA, Gelboin HV and Gonzalez FJ (1990) The human CYP2F gene subfamily: identification of a cDNA encoding a new cytochrome P450, cDNA-directed expression, and chromosome mapping. *Biochemistry* **29**:5491-5499.

Plopper CG, Chang AM, Pang A and Buckpitt AR (1991) Use of microdissected airways to define metabolism and cytotoxicity in murine bronchiolar epithelium. *Exp Lung Res* **17**:197-212.

Plopper CG, Suverkropp C, Morin D, Nishio S and Buckpitt A (1992) Relationship of cytochrome P-450 activity to Clara cell cytotoxicity. I. Histopathologic comparison of the respiratory tract of mice, rats and hamsters after parenteral administration of naphthalene. *J Pharmacol Exp Ther* **261**:353-363.

Plopper CG (1993) Pulmonary bronchiolar epithelial cytotoxicity: microanatomical considerations, in *Metabolic Activation and Toxicity of Chemical Agents to Lung Tissue and Cells* (Gram TE ed) pp 1-24, Pergamon Press, New York.

Ritter JK, Owens IS, Negishi M, Nagata K, Sheen YY, Gillette JR and Sasame HA (1991) Mouse pulmonary cytochrome P-450 naphthalene hydroxylase: cDNA cloning, sequence, and expression in Saccharomyces cerevisiae. *Biochemistry* **30**:11430-11437.

Schenkman, JB and Jansson, I (1999) Measurement of Cytochrome P-450, in *Current Protocols in Toxicology* (Maines, MD ed) pp 4.1.1-4.1.14, Wiley & Sons, Hoboken.

Shevchenko A, Wilm M, Vorm O and Mann M (1996) Mass spectrometric sequencing of proteins from silver-stained polyacrylamide gels. *Anal Chem* **68**:850-858.

Shultz MA, Choudary PV and Buckpitt AR (1999) Role of murine cytochrome P-450 2F2 in metabolic activation of naphthalene and metabolism of other xenobiotics. *J Pharmacol Exp Ther* **290**:281-288.

Stone KC, Mercer RR, Freeman BA, Chang LY and Crapo JD (1992) Distribution of lung cell numbers and volumes between alveolar and nonalveolar tissue. *Am Rev Respir Dis* **146**:454-456.

Su T, Bao Z, Zhang QY, Smith TJ, Hong JY and Ding X (2000) Human cytochrome P450 CYP2A13: predominant expression in the respiratory tract and its high efficiency metabolic activation of a tobacco-specific carcinogen, 4-(methylnitrosamino)-1-(3-pyridyl)-1-butanone. *Cancer Res* **60**:5074-5079.

Thornton-Manning JR and Dahl AR (1997a) Metabolic capacity of nasal tissue interspecies comparisons of xenobiotic-metabolizing enzymes. *Mutat Res* **380**:43-59.

Thornton-Manning JR, Nikula KJ, Hotchkiss JA, Avila KJ, Rohrbacher KD, Ding X and Dahl AR (1997b) Nasal cytochrome P450 2A: identification, regional localization, and metabolic activity toward hexamethylphosphoramide, a known nasal carcinogen. *Toxicol Appl Pharmacol* **142**:22-30.

West JA, Pakehham G, Morin D, Fleschner CA, Buckpitt AR and Plopper CG (2001) Inhaled naphthalene causes dose dependent Clara cell cytotoxicity in mice but not in rats. *Toxicol Appl Pharmacol* **173**:114-119.

Zupko K, Poria Y and Lancet D (1991) Immunolocalization of cytochromes P-450olf1 and P-450olf2 in rat olfactory mucosa. *Eur J Biochem* **196**:51-58.

Footnotes

[2]Molecular Structure Facility

University of California, Davis

[3]Department of Anatomy, Physiology, and Cell Biology

School of Veterinary Medicine

University of California, Davis

Supported by NIEHS grants ES08408, ES04311, ES06700, ES04699, and NCRR RR00169.

The University of California at Davis is an NIEHS Center (05707) and support for core facilities used in this work is gratefully acknowledged.

Reprint Requests

R. Michael Baldwin

Veterinary Medicine: Molecular Biosciences

1311 Haring Hall

UC Davis

Davis, CA 95616

Figure 1

Northern blot comparison of lung, liver, and kidney from rat (30 μg of total RNA) and mouse (5 μg of total RNA).

a) Blots were hybridized with ^{33}P-labeled CYP2F4 and rat GADPH probes.

b) Quantification by phosphor-imaging and image analysis. Results are expressed as area units of CYP2F / GAPDH (mean ± SD, n=4). Using a two-tailed heteroscedastic *t* test, transcript levels were found to differ significantly across species in lung ($p<0.01$), liver ($p<0.01$) and kidney ($p<0.05$). Within each species, differences in transcript levels across tissues also proved significant ($p<0.01$ for all comparisons).

Figure 2

Relative affinity estimation of the rabbit anti-CYP2F2 polyclonal antibody for rCYP2F2 and rCYP2F4 using a dilution series of rCYP2F expressing insect cell lysates.

"*" denotes samples outside of the calculated linear range.

a) Total protein stained with Sypro Ruby (Molecular Probes). RFU areas of the protein band associated with expressed rCYP2F (arrows) were quantified with ImageQuant 5.1. Comparison of slopes (RFU area / ng cell lysate) yielded a rCYP2F2 / rCYP2F4 slope ratio of 0.67

b) Immunoblot analysis using the anti-CYP2F2 polyclonal antibody, yielding a rCYP2F2 / rCYP2F4 slope ratio of 0.65.

Figure 3

Immunoblot of liver post mitochondrial supernatants from mouse (13 μg total protein) and rat (9 μg total protein). Recombinant CYP2F4 was used as both a positive control and molecular weight standard.

Figure 4

Immunoblot of an airway subcompartment (minor daughter airways) using the rabbit anti-CYP2F2 polyclonal antibody. The total amount of cellular protein loaded for each species is reported along with the relative amount of each standard used for blot-to-blot comparisons. Inset- linear regression analysis of quantified standards. All samples were diluted to fall within the linear range defined by the standards.

Figure 5

Immunoblot of mouse and rat nasal subcompartments using the rabbit anti-CYP2F2 polyclonal antibody. The total amount of cellular protein loaded for each region is reported. No other immunoreactive bands were observed outside of the blot regions shown.

Figure 6

Summary of immunoblot analysis of mouse and rat airways and nasal subcompartments. Results reported as mean ± SD (n=5). Units are arbitrary and derived from normalization using the four internal standards. In all instances tissue expression levels of CYP2F differed significantly between mouse and rat (two-tailed heteroscedastic *t* test, $p<0.01$).

Inset- Magnification of rat lung CYP2F expression levels.

Figure 7

Immunoblot of rhesus macaque nasal tissue (30 μg of total cellular protein) using the rabbit anti-CYP2F2 polyclonal antibody. The two most concentrated rCYP2F4 standards were non-linear (NL) and not used in regression analysis.

Inset- Comparative CYP2F expression levels in ethmoturbinates of monkey (n=3), rat (n=5), and mouse (n=5). Results reported as mean ± SD using arbitrary units standardized for comparison to Figure 6. All three mean values were significantly different (two-tailed heteroscedastic *t* test, $p<0.001$).

Figure 8

Identification of immunoreactive proteins using peptide mass fingerprinting of electrophoresed ethmoturbinate microsomal protein from mice, rats, and rhesus macaque.

a) Coomassie blue-stained polyacrylamide gel. Arrows denote excised bands (line demarcated in monkey sample).
b) Immunoblot using rabbit anti-CYP2F2 polyclonal antibody. Each sample contains 10 micrograms of microsomal protein. Solid bars denote protein molecular weight markers used for alignment of the immunoreactive bands with the corresponding regions on the Coomassie blue-stained gel.

JPET Fast Forward. Published on January 14, 2004 as DOI: 10.1124/jpet.103.062901
This article has not been copyedited and formatted. The final version may differ from this version.

Table 1

Cytochrome P450 Proteins Identified by Peptide Mass Fingerprinting

Species	*Band*	*CYP Isoform*	*SWISS-PROT Accession*	*Molecular Weight*	*Peptide Matches*	*Sequence Coverage*	*Unique Matches**
Rat	Upper	CYP2A3	P20812	56510	12	29 %	11
		CYP2G1	P10610	56781	8	20 %	7
	Lower	CYP2F4	O35293	55946	10	24 %	8
		CYP2A3	P20812	56510	7	17 %	5
Mouse	Upper	CYP2A5	P20852	56741	16	39 %	16
		CYP2G1	Q9WV19	56820	10	25%	10
	Lower	CYP2A5	P20852	56741	9	22 %	8
		CYP2F2	P33267	55949	8	23 %	7
Rhesus	Upper	CYP2A13	Q16696	56674	9	20 %	5
		CYP2A6	P11509	56541	6	15 %	2
		*CYP2J2***	*P51589*	*57611*	*4*	*9 %*	*3*
		*CYP2F1***	*P24903*	*55499*	*2*	*5 %*	*2*
	Lower	CYP2A13	Q16696	56674	6	19 %	6

Cytochrome P450 proteins identified by peptide mass fingerprinting/mapping in ethmoturbinate microsomes.

*denotes peptide fragments matching only the isoform listed

**Tentative identifications due to insufficient number of matched peptide fragments

JPET Fast Forward. Published on January 14, 2004 as DOI: 10.1124/jpet.103.062901

1A

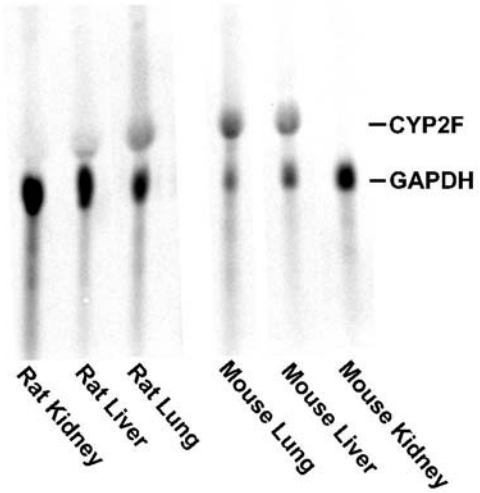

JPET Fast Forward. Published on January 14, 2004 as DOI: 10.1124/jpet.103.062901
This article has not been copyedited and formatted. The final version may differ from this version.

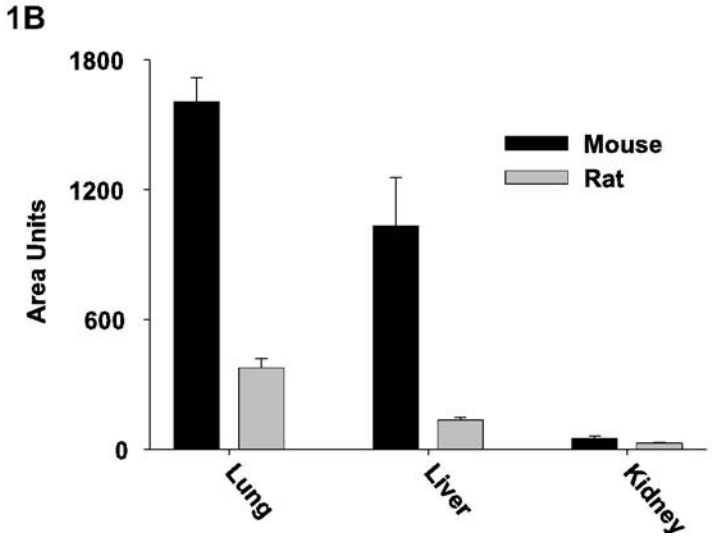

JPET Fast Forward. Published on January 14, 2004 as DOI: 10.1124/jpet.103.062901

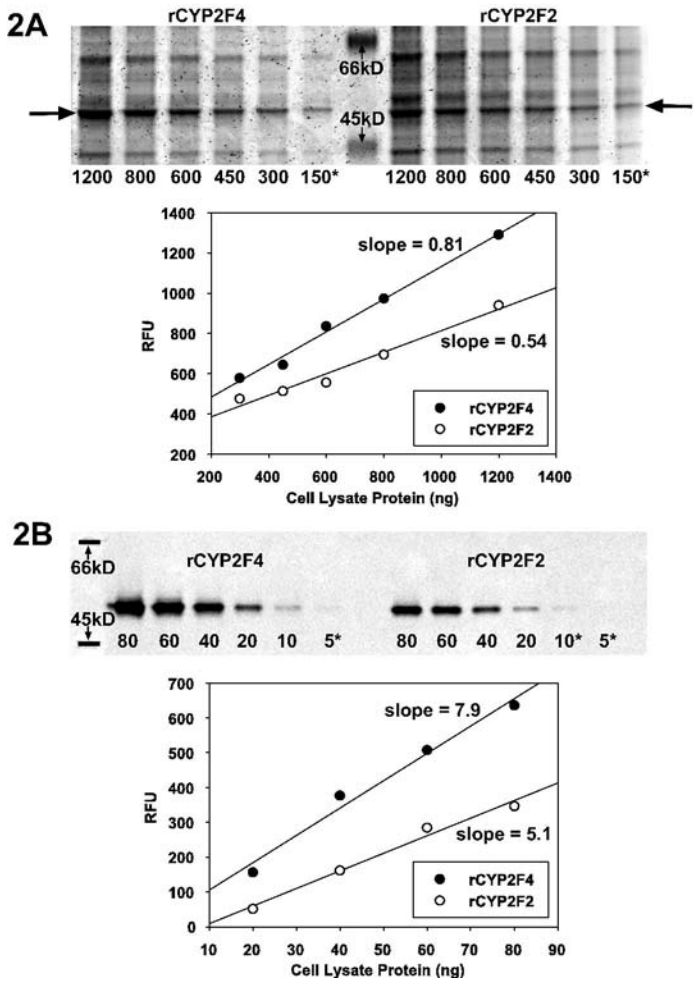

JPET Fast Forward. Published on January 14, 2004 as DOI: 10.1124/jpet.103.062901
This article has not been copyedited and formatted. The final version may differ from this version.

3

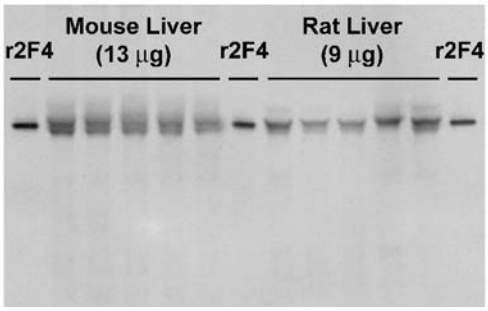

JPET Fast Forward. Published on January 14, 2004 as DOI: 10.1124/jpet.103.062901

4

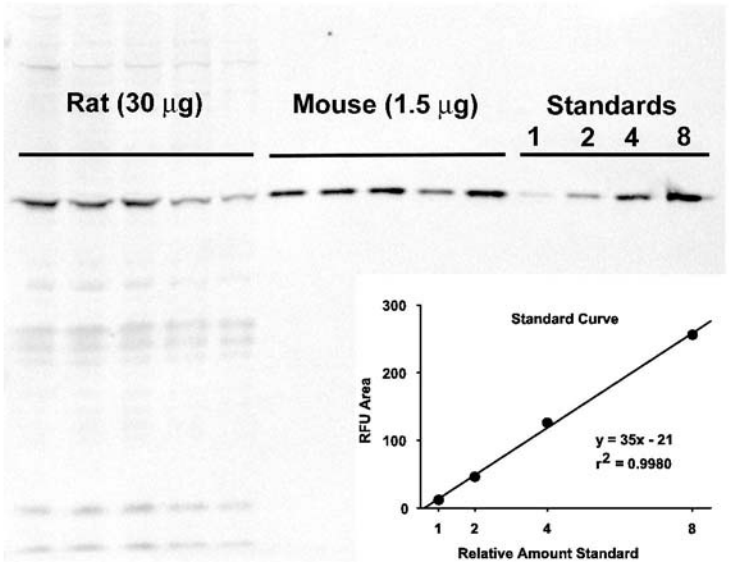

JPET Fast Forward. Published on January 14, 2004 as DOI: 10.1124/jpet.103.062901
This article has not been copyedited and formatted. The final version may differ from this version.

5

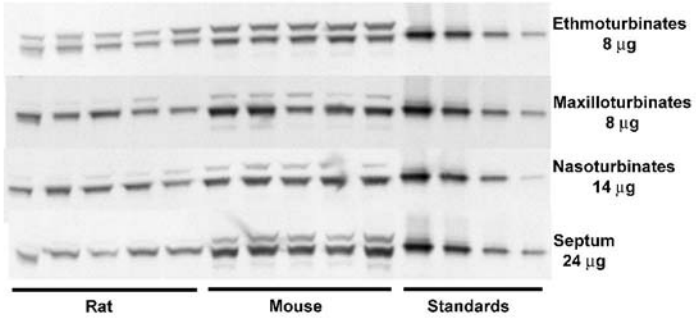

JPET Fast Forward. Published on January 14, 2004 as DOI: 10.1124/jpet.103.062901

6

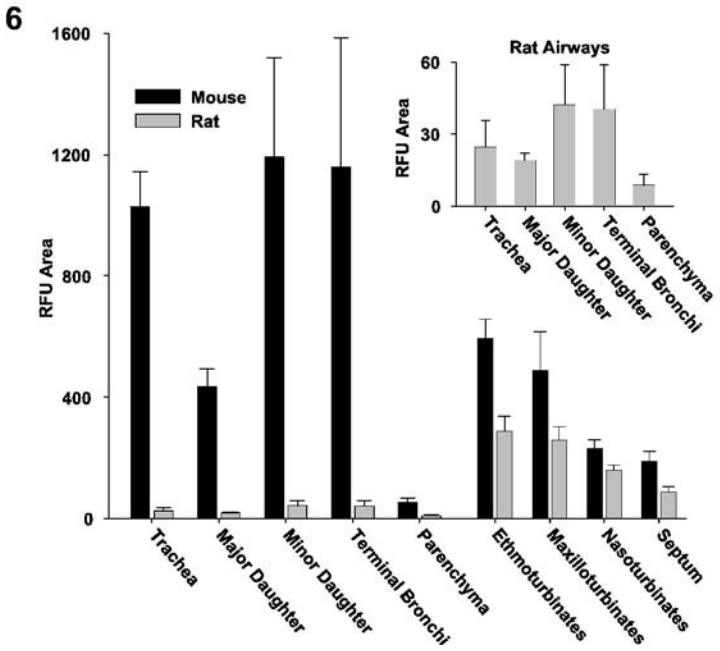

JPET Fast Forward. Published on January 14, 2004 as DOI: 10.1124/jpet.103.062901

7

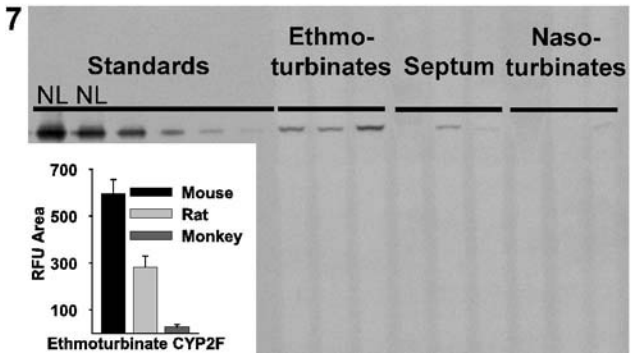

JPET Fast Forward. Published on January 14, 2004 as DOI: 10.1124/jpet.103.062901

8